# Role of Water Mediated Interactions in Calcium-Coupled Allostery of Calmodulin Domains

Cheng Tan,[†,‡] Wenfei Li,[†,‡] Wei Wang,[*,†,‡] and Dave Thirumalai[*,¶]

†*National Laboratory of Solid State Microstructure and Department of Physics, Nanjing University, 210093, China*

‡*Collaborative Innovation Center of Advanced Microstructures, Nanjing University, Nanjing 210093, China*

¶*Department of Chemistry, University of Texas, Austin, TX, 78712 USA*

E-mail: wangwei@nju.edu.cn; dave.thirumalai@gmail.com

**Abstract**

Allosteric communication between distant parts of protein controls many cellular functions. Binding of $Ca^{2+}$ to the helix-loop-helix motifs (termed EF-hands) in calmodulin (CaM) leads to large conformational changes poising it for the binding of target proteins involved in variety of cell signaling events. Despite the physiological importance, the mechanism of $Ca^{2+}$-mediated allosteric transitions in CaM remains elusive. Particularly, it is still unclear how water molecules contribute to $Ca^{2+}$ coordination and the coupled conformational motions. We use all-atom molecular dynamics simulations with enhanced sampling method to investigate the coupling between the $Ca^{2+}$ binding, dehydration, and the conformational change of the isolated CaM domains, each containing two EF-hands. We reveal a water-bridged coordination mechanism during $Ca^{2+}$ binding and dehydration, in which the bridging water molecules

reduce the entropy penalty during the coordination of liganding residues, thus contributing to efficient ligand binding in CaM domains. Exposure of hydrophobic sites occurs by calcium induced rotation of the helices of EF-hands with the hydrophobic core serving as the pivot. Interestingly, we find that despite being structurally similar, the structural response in the two EF-hands upon $Ca^{2+}$ binding is highly asymmetric, which is needed for allosteric communication between them. The atomically detailed picture for the allosteric transitions of the CaM EF-hands, which are the first events in mediating a variety of intracellular processes, reveal the complex interplay between the discrete water molecules, dehydration of $Ca^{2+}$, and CaM structural changes.

**Keywords**: Allosteric transition, metadynamics, EF-hands, water-mediated coordination, Calmodulin.

# Introduction

Calmodulin (CaM), a versatile calcium ($Ca^{2+}$) sensing protein expressed in all eukaryotic cells, is involved in a bewildering range of intracellular signaling processes.[1] Examples include activation of kinases,[2] muscle contraction,[3] gene regulation,[4] signal transduction,[5] and apoptosis.[6] Binding of $Ca^{2+}$, whose intracellular and extracellular concentrations differ by several orders of magnitude, to CaM results in a large conformational change leading to the exposure of hydrophobic residues that serve as recognition sites for target proteins. CaM is composed of two nearly symmetric globular domains connected by a flexible central helix.[7,8] Each domain consists of two helix-loop-helix motifs, termed EF-hands, (Fig. 1A,B), which are found in a large number of calcium-sensing proteins.[9,10] The EF-hands chelate $Ca^{2+}$, resulting in coordination to seven ligands arranged in a pentagonal bipyramid geometry (often involving one water molecule and five liganding residues) with the negatively charged residues in the loop[10] (Fig.1C,E). In the apo state of CaM (Fig. 1B,D), the helices in the EF-hand motif are arranged in an anti-parallel manner. Upon binding of $Ca^{2+}$, the helices undergo substantial rearrangement into a nearly perpendicular conformation, exposing the hydrophobic sites which enable recognition and subsequent activation of target proteins.[9,11,12] Through such a mechanism, CaM initiates a variety of cellular processes.

In a more general context, $Ca^{2+}$-triggered conformational changes in CaM is an example of allostery, which describes the structural changes that occur in enzymes and molecular machines at distances far from the site at which a ligand binds.[13,14] Nature utilizes such functional motions, which are triggered by binding of cofactors, such as metal ions, ATP, and other small molecules to specific sites in proteins and RNA, to execute a variety of functions.[15–21] Binding of cofactors at a certain site (allosteric site) induces structural rearrangements at a distant site (regulated site) in the enzyme, thereby modulating the downstream activity. By such allosteric movements, small local changes are amplified over long distances, which allow for control and regulation of cellular signaling and functions.[22,23] Despite the biological importance of allostery, some key questions are still not fully understood, includ-

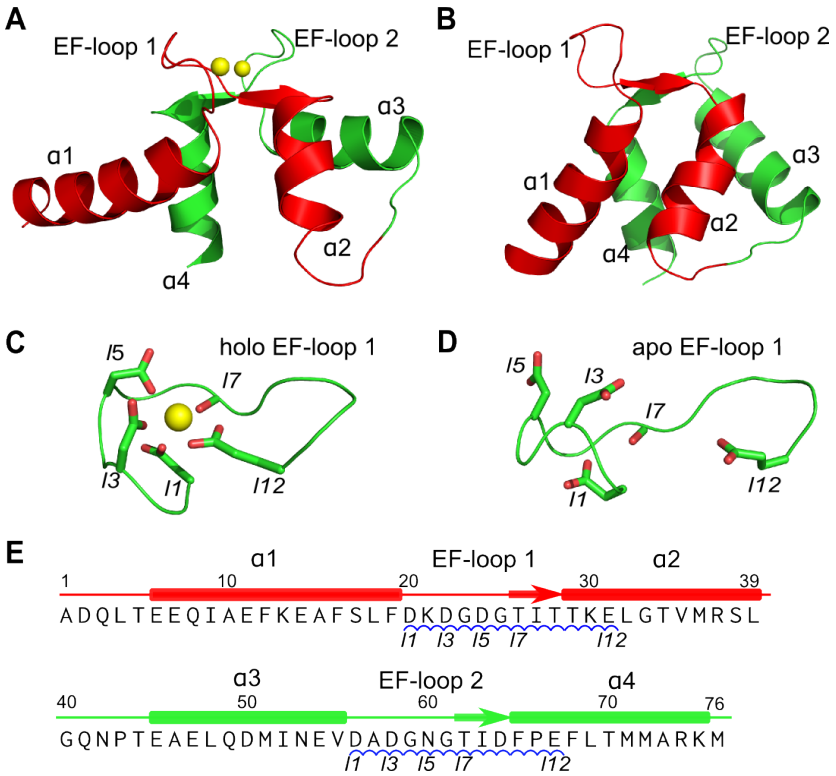


Figure 1: Structure and sequence of nCaM and the $Ca^{2+}$ binding EF-loops. (A, B) Structure of nCaM in the holo state (A) and apo state (B). Helix-loop-helix motifs $\alpha 1$–EF-loop1–$\alpha 2$ (red) and $\alpha 3$–EF-loop2–$\alpha 4$ (green) comprise two EF-hands in the N-terminal domain of Calmodulin. $Ca^{2+}$ ions are colored yellow. (C, D) Conformation of EF-loop 1 in the holo state (C) and apo state (D). (E) The sequence of nCaM and corresponding secondary structures. $Ca^{2+}$ binding loops are underlined with blue wavy lines. In (C) (D) and (E), the native ligands are marked with "$l - n$" to indicate their position in the EF-loop.

ing: i) How do the cofactors bind to the allosteric sites and regulate the conformational changes? ii) What physical interactions enable the propagations of the allosteric signal? iii) How do water molecules contribute to the cofactor binding and the conformational motions? Because of the rich experimental data and the typical allosteric feature, CaM is an ideal system for answering these questions computationally.[24? ? –33] For example, a recent simulation work using atomistic molecular dynamics (MD) and Markov state models revealed the conformational heterogeneity of the calmodulin binding interface which may facilitate the recognition of diverse targets.[?]

Experiments have characterized the kinetics of conformational changes in CaM domains upon $Ca^{2+}$ binding.[28,34–45] For example, mutation experiments, in which the N-terminal domain of CaM (nCaM) is locked in the closed conformation by a disulfide bond, was used to propose that the glutamic acid at position 12 (Fig.1E) of the EF-loop is responsible for the conformational transition in response to the binding of $Ca^{2+}$ by a two-step mechanism.[45] In the first step, the $Ca^{2+}$ binds to the N-terminal part of the EF-loop; then in the second step, the glutamic acid at position 12 is coordinated to $Ca^{2+}$ and induces the conformational transition through hinge rotation of the isoleucine in the eighth position of the loop.[45] However, due to the temporal and spatial resolution limits, direct observation of the conformational changes in CaM triggered by $Ca^{2+}$ at atomic level is still lacking. Particularly, it is not clear how the water molecules are involved in the $Ca^{2+}$ coordination and the accompanied allosteric coupling.

Here, we used the bias-exchange metadynamics method[46] to investigate the $Ca^{2+}$ binding coupled conformational changes of CaM domains by explicitly modeling $Ca^{2+}$ in the simulations. Such MD can present a detailed picture of the allosteric motions of CaM provided that the conformational space can be adequately sampled.[8,28,47–49] For a direct comparison with the above mentioned experiment,[45] our discussions mainly focused on the nCaM. However, similar simulations were also conducted for the C-terminal domain of CaM (cCaM), for which a number of spectroscopy data are available and can be used for benchmark. We

extracted the full free energy landscape of the $Ca^{2+}$ coupled conformational changes of CaM domains at atomic level.

Our results revealed a water-bridged coordination mechanism for the $Ca^{2+}$ binding process, in which the water molecules reduce the dehydration entropy penalty. This enables efficient $Ca^{2+}$-ligand coordination and allosteric motions of the nCaM. We propose that the water-bridged coordination may be general mechanism employed in metal-coupled folding and allosteric communication in proteins. We also showed that $Ca^{2+}$ binding leads to rotation of the EF-hand helices with the hydrophobic core as the pivot, a structural change that should precede recognition by target proteins for signal transduction. In addition, our results revealed obvious asymmetry in the allosteric coupling of the paired EF-hands: the EF-hand 1 ($EF_1$) binds $Ca^{2+}$ in a sequential manner by chelating to the N-terminal residues followed by coordination with the central residues, and finally to the C-terminal residues. In contrast, chelation of $Ca^{2+}$ to the EF-hand 2 ($EF_2$) is initiated either to the residues in the N- and/or C-terminal residues followed by coordination to the central residues. Similar results were obtained for the cCaM.

# Results and Discussion

## $Ca^{2+}$ binding is coupled to conformational changes of the EF-hand motifs

We use well-tempered bias-exchange metadynamics[46,50] and the corresponding reweighting techniques[51] to extract the free energy landscape projected onto physically motivated multi-dimensional reaction coordinates characterizing $Ca^{2+}$ binding and the conformational change. Quantitative analysis of the changes in these coordinates allows us to infer the mechanism of coupling between $Ca^{2+}$ binding, the role of water, and the allosteric conformational changes in calmodulin. In particular, we use the "path collective variables" $S_\alpha$ ($\alpha = 1, 2, 3$, and 4), defined in the **Methods** section, to describe the conformational changes of the two EF-hand

motifs. Small and large values of $S_\alpha$ correspond to open and closed states, respectively. In order to assess the consequences of $Ca^{2+}$ binding, we use the native coordination numbers $N_\alpha$ (see **Methods** for definition), representing the number of native ligands (oxygen atoms of residues that are coordinated with $Ca^{2+}$ in the native holo structure) that bind to $Ca^{2+}$ during the allosteric transitions for the two EF-hand motifs, respectively. Figure 2 shows the free energy landscapes, $F(N_1, S_1)$ and $F(N_2, S_2)$, of the nCaM. For both $EF_1$ and $EF_2$, the conformational change of nCaM is tightly coupled to the extent of $Ca^{2+}$ binding as indicated by the conformational distributions at different $N_1$ and $N_2$ values. When $S_\alpha$ ($\alpha = 1$ or 2) is large and $N_\alpha$ ($\alpha = 1$ or 2) is small, the closed state is more stable whereas when the native ligands are fully coordinated to $Ca^{2+}$ the open structure is more stable (Fig. 2A,B). Interestingly, even with full coordination of native ligands ($N_1 = N_2 = 6$) to $Ca^{2+}$, the two EF-hands sample a wide range of conformations as assessed by $S_1$ and $S_2$ fluctuations, suggesting the conformational plasticity of the open state. Conformational plasticity for the $Ca^{2+}$ bound state, which was also observed in experiments, could be the major reason that the EF-hand motifs recognize and bind a variety of target proteins.[52,53] The free energy landscapes for the cCaM are mostly similar to those of the nCaM except for one crucial difference, namely, even in the case of low coordination number, both EF-hands in the cCaM can adopt an open conformation, suggesting higher flexibility of the cCaM (Fig.S1). Interestingly, previous NMR studies have showed that the open conformation can have a minor but significant population ($5 - 10\%$) even without $Ca^{2+}$ binding,[34,54] which is in accordance with our simulation results.

Although the two EF-hand motifs have similar structures, comparison of Fig. 2A and Fig. 2B shows that there are noticeable differences in the free energy landscapes upon $Ca^{2+}$ binding. For example, when three or four ligands bind to $Ca^{2+}$, the conformation of $EF_1$ is poised to make a transition to the open structure. When $N_1$ exceeds $\sim 4$ the fully closed structure is rarely sampled (Fig. 2A). In contrast, $EF_2$ visits a much larger conformational space ranging from the fully open state to the fully closed state, even when $N_2$ exceeds 3

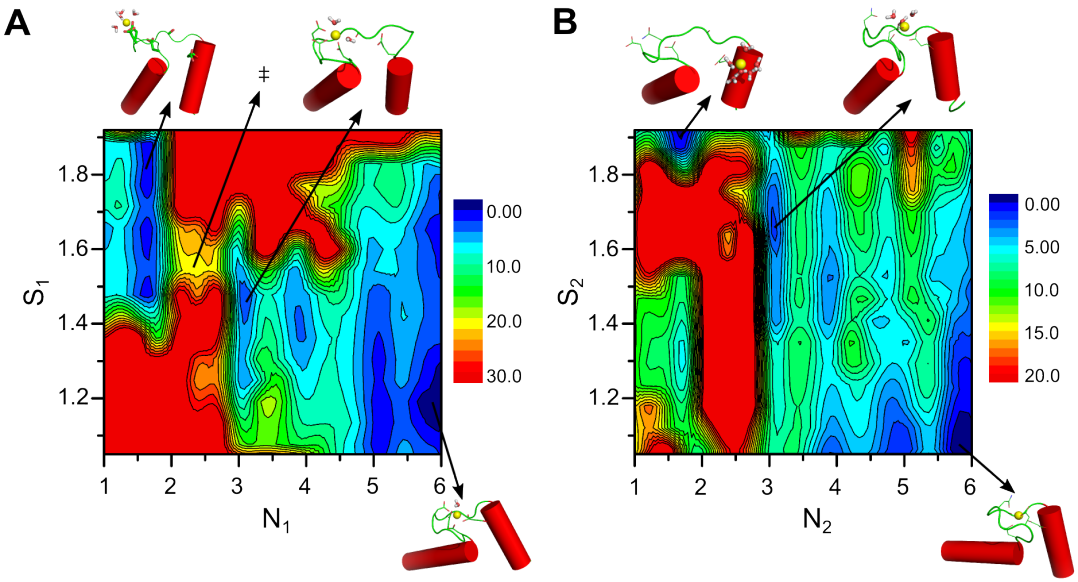


Figure 2: Free energy profiles of the $Ca^{2+}$ coupled conformational transitions of $EF_1$ (A) and $EF_2$ (B) projected onto the collective variables ($N_1$, $S_1$) and ($N_2$, $S_2$), respectively. Representative conformations of the major basins in the landscape are also shown. The unit of the free energy is kcal/mol.

or 4 (Fig.2B). These differences in the allosteric features are reasonable since the two EF-hand motifs have different amino-acid sequences in the $Ca^{2+}$ binding loop. Consequently, the ensembles of structures with three or four native ligands bound to the $Ca^{2+}$ have large differences in the two EF-motifs, which could play an important role in signaling. Most interestingly, in $EF_2$ there is a region when $S_2$ is small corresponding to the open structure but with small $N_2$ value (Fig. 2B). Detailed analysis (see Supplementary Fig.S2 online) shows that the open conformation of $EF_2$ can only be stabilized when $EF_1$ is also in the open conformation with most of its native ligands bound to $Ca^{2+}$ ($N_1 \geq 5$). Thus, the behavior of $EF_2$ is affected by the conformation of $EF_1$ through long range allosteric interactions between the two EF-hands, which will be discussed later in more details.

## Step-wise dehydration of $Ca^{2+}$ and ligand formation are cooperatively coupled

Our metadynamics simulations allow us to construct the changes in the coordination states of $Ca^{2+}$, including the role that water and potential non-native ligands (those that are not present in the native open structure) play during the closed $\rightarrow$ open transition. Figure 3 shows the average of the total coordination number, $N_T$ (sum of the number of water molecules and the number of ligands bound to $Ca^{2+}$), as a function of $N_\alpha$ ($\alpha = 1, 2$) for the nCaM. At a low value of $N_1$ (Fig. 3A), approximately six water molecules are coordinated to $Ca^{2+}$. As $N_1$ increases, water molecules are expelled, showing that dehydration occurs in steps. The number of water molecules expelled from $Ca^{2+}$ and replaced by native ligands depends on $N_1$. Upon binding of ligands ($N_1 = 1$) $Ca^{2+}$ loses a single water molecule whereas two water molecules are ejected when $N_1 = 3$ (Fig. 3A). The decrease in the number of water molecules by two when $N_1 = 3$ represents coordination of $Ca^{2+}$ to negatively charged residues (Asp20, Asp22 and Asp24) at the N-terminal of the loop (see Supplementary Fig.S3 online). In the free energy landscape the decrease represents a major barrier in the closed to open transition (see yellow region with label ‡ in Fig. 2A). In the holo state ($N_1 = 6$), only one water molecule is bound to the $Ca^{2+}$, which makes the coordination number saturate at $N_T = 7$.

A similar process, with one crucial difference, occurs as $Ca^{2+}$ coordination drives the conformational changes in $EF_2$. During the binding of the native ligands ($N_2 \leq 3$ in Fig. 3B) $Ca^{2+}$ becomes transiently coordinated to non-native ligands, notably the side-chain oxygen atoms of Asp64. The carboxylic oxygen of Asp64 has a probability of $\sim 0.52$ to come into the first ligand shell of $Ca^{2+}$ when $N_2 = 3$ (see Table 1 and Fig. 3C; the probability of the coordination is defined in the **Methods** section). As the binding process and conformational changes proceed further, the non-native ligands (oxygen atoms from Asp64) are replaced by the native ligands. Figures 3C,D explicitly show that non-native coordination of Asp64–$Ca^{2+}$ is replaced by Asn60–$Ca^{2+}$, a ligand present in the native holo state. Such miss-ligation and

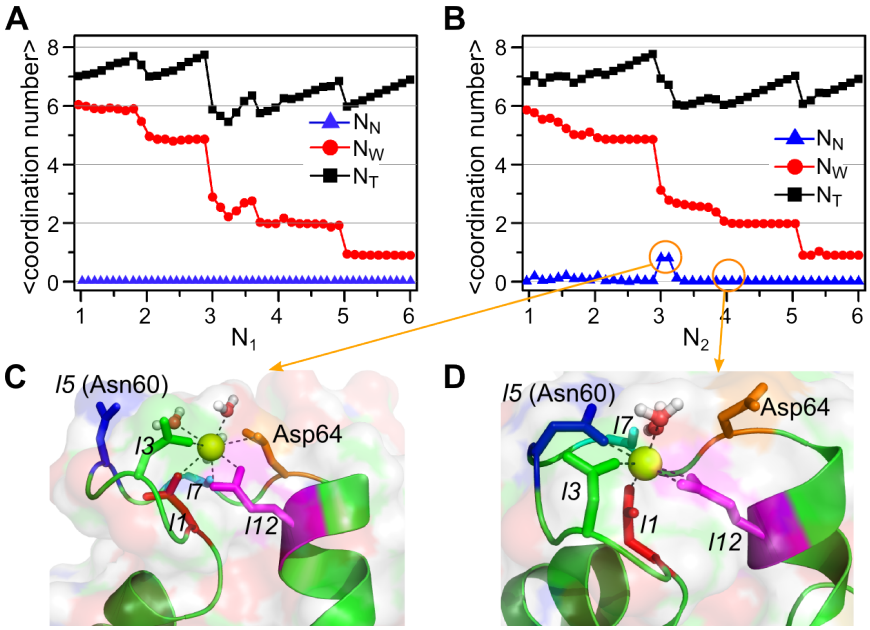


Figure 3: Number of coordinated water molecules ($N_W$), non-native ligands ($N_N$) as well as the total coordination number ($N_T$) as functions of $N_1$ and $N_2$ for $EF_1$ (A) and $EF_2$ (B). (C) The non-native ligand Asp64 (orange) coordinated to $Ca^{2+}$ when $N_2 = 3$. (D) When $N_2 = 4$, Asn60 ($l5$, blue) is coordinated to $Ca^{2+}$, and the bond formed by Asp64 and $Ca^{2+}$ is broken.

ligand-exchange have been proposed and observed in a number of experiments and MD simulations of other metalloproteins.[55–57] These processes may be necessary to minimize the free energy cost caused by the sharp dehydration of metal ion during the binding process.[56,57]

## Molecular mechanism of the $Ca^{2+}$ binding

The results presented above strongly suggest that the conformational changes in the nCaM are coupled to the binding of $Ca^{2+}$ with water playing a crucial role. Therefore, it is of interest to further clarify the order of binding of residues that are coordinated to $Ca^{2+}$ in detail. Due to the nature of the metadynamics simulations, the kinetic information can only be indirectly gleaned using the present simulations. In particular, we can approximately extract the binding order based on the correlation analysis, as done in previous studies.[56,58]

*Binding to $EF_1$:* Figure 4A shows the coordination probability, $P(i, \overline{N_\alpha})$, (defined in **Methods** section) for each ligand bound to the $Ca^{2+}$ ion in the native state with the total

native coordination number being one to six for the $EF_1$ of nCaM. Using $P(i, \overline{N_\alpha})$ we can extract the binding order of the native ligands of $EF_1$ to $Ca^{2+}$. The representative structures are also shown for each coordination conformation (Fig. 4B). Similar results for $EF_2$ are shown in Fig. 4C,D. For the $EF_1$, the first one or two native ligands bound to $Ca^{2+}$ can be either the N-terminal part (Asp22 or Asp24, at the third or fifth position), or the C-terminal part (Glu31, at the twelfth position) of the EF-loop. This observation is not surprising since negatively charged states of these residues contribute to the preferred binding and localization of the $Ca^{2+}$. Furthermore, these residues mostly point outward to the solvent in the apo state. However, the other two native ligands associated with residues Asp20 and Thr26 are relatively buried inside the protein. Interestingly, the three residues that are coordinated to the $Ca^{2+}$ when $N_1 = 3$ are predominantly the negatively charged residues Asp20, Asp22, and Asp24 located at the N-terminal of the EF-loop. These results suggest that when the $Ca^{2+}$ is first coordinated to Glu31 at the C-terminus of the EF-loop, there is a substantial probability of rupture with subsequent solvation, or less likely, transfer to the more negatively charged N-terminal part. This process results in a large enthalpy change for the disassociation of Glu31 and $Ca^{2+}$, which may contribute to the high free energy barrier between $N_1 = 2$ and $N_1 = 3$ shown in Fig. 2A.

Another possible reason for such a high free energy barrier is the dehydration of $Ca^{2+}$ involving rupture of several coordination bonds between the $Ca^{2+}$ and water molecules.[59,60] The fourth native ligand coordinated to $Ca^{2+}$ in $EF_1$ is the backbone oxygen of Thr26, which is at the central part of the EF-loop. Binding of $Ca^{2+}$ to Thr26 results in the formation of a water-bridged interaction between Glu31 and $Ca^{2+}$. In this structure, the oxygen of the water molecule is coordinated to $Ca^{2+}$ as a ligand. At the same time, it forms a hydrogen bond with the side-chain oxygen from Glu31 (Fig. 4B). We note that such a water-bridged coordination structure is quite similar to the intermediate structure identified in experiments.[45] When the bridging water is finally expelled, the last two native ligands, side-chain oxygen atoms from Glu31, are coordinated to $Ca^{2+}$. Overall, our results indicate a stepwise

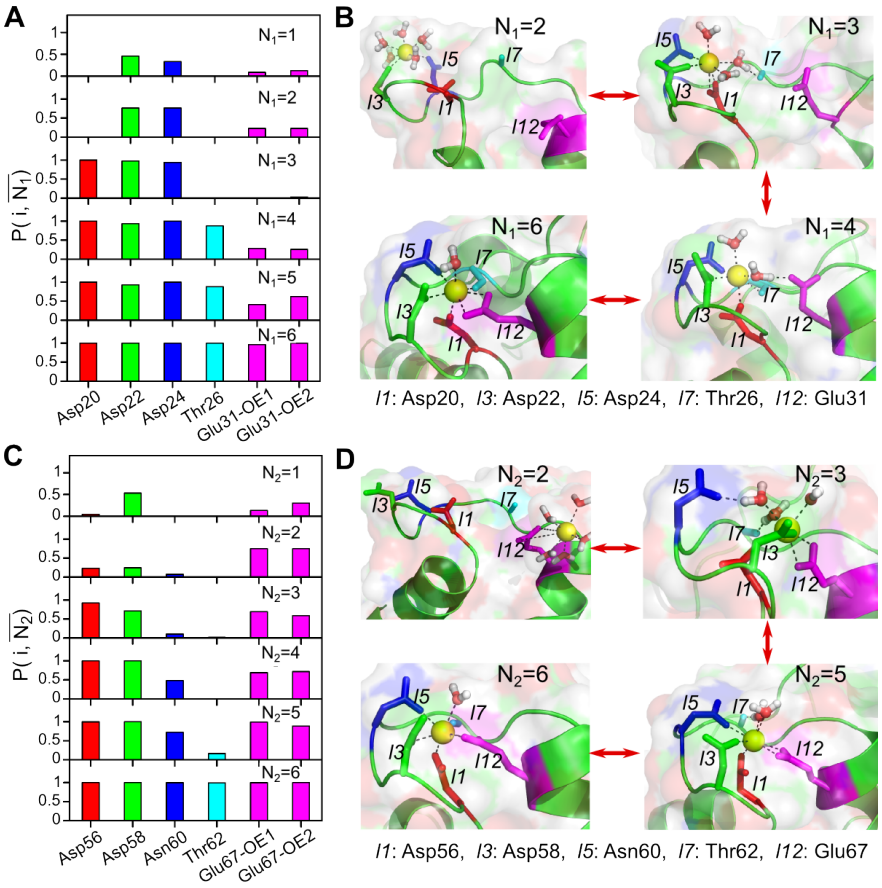


Figure 4: The $Ca^{2+}$ binding sequence of $EF_1$ and $EF_2$. (A) Coordination probability $P(i, \overline{N_\alpha})$ for the six native liganding residues of $EF_1$. Different liganding residues are colored in different colors. (B) Schematic representations of the binding process of the native ligands. (C) and (D) show the binding sequence of the $EF_2$.

binding of $Ca^{2+}$ to $EF_1$: first, $Ca^{2+}$ is captured by an acidic residue (most probably Asp22); subsequently, the N-terminal part of the EF-loop plays a role in further coordination to $Ca^{2+}$, establishing some links between the incoming helix and the central $\beta$ strands; finally, Thr26 and Glu31 are sequentially captured and bound to the $Ca^{2+}$, leading to the native structure. The order of binding of $Ca^{2+}$ to the residues predicted in our simulations is consistent with the two-step $Ca^{2+}$ binding mechanism proposed based on crystal structure of a mutant.[11,45] Interestingly, the results in Fig. 2 and Fig. 4 show that once the two oxygen atoms from Glu31 are coordinated to $Ca^{2+}$, the most stable conformation of $EF_1$ switches to the open form, suggesting the crucial role of the highly conserved Glutamic acid at the $12^{th}$ position in the $Ca^{2+}$ binding coupled conformational transition of nCaM.[11,34,45] A very recent work combining nuclear magnetic resonance measurements and molecular dynamics simulations also suggested the important role of the bidentate ligand Glu140 on the $Ca^{2+}$ coupled conformational motions of the cCaM.[44]

*Binding to $EF_2$:* The mechanism of binding of $Ca^{2+}$ to $EF_2$ is dramatically different (Fig. 4C,D). Instead of binding to the native ligands by the sequence of N-terminal residues $\rightarrow$ central residues $\rightarrow$ C-terminal residues as in $EF_1$, the $Ca^{2+}$ binds initially to the N-terminal residues Asp56, Asp58 (or C-terminal residues Glu67), which is followed by the binding of the C-terminal residues Glu67 (or N-terminal residues Asp56, Asp58). Only at the final stage, it is bound to the central residues Asn60 and Thr62. Therefore, the $Ca^{2+}$ binding to the $EF_2$ follows the sequence N-terminal and/or C-terminal residues $\rightarrow$ central residues. The differing mechanism of coordination to $Ca^{2+}$ probably arises from the divergence of their amino-acid sequences. For example, the "central" residues (especially at the $5^{th}$ position) in $EF_1$ are more negatively charged compared to those in $EF_2$. Consequently, coordination of these residues to $Ca^{2+}$ occurs at a relatively early stage.

We also found that before $Ca^{2+}$ binds to the central residues Asn60 and Thr62, a non-native ligand Asp64 is coordinated with $Ca^{2+}$ (Fig. 3B,C and D). Consequently, the last steps of the $Ca^{2+}$ binding to $EF_2$ must involve ligand exchange between the non-native ligands

and the native ligands. Interestingly, during the ligand exchange, water molecules bridge the $Ca^{2+}$ and the native ligands. As we show below, water mediated coordination reduces the free energy barrier of the formation of native coordination bonds. For $EF_2$, the water molecules were found during the formation of coordination of $Ca^{2+}$–Asn60 and $Ca^{2+}$–Thr62, which is consistent with the observation that there is a tendency to capture an extra water molecule as a ligand leading to a decreased contribution for the backbone oxygen of Thr62.[48] In experiments,[45] Asp64 was mutated to Asn64 for the $EF_2$. Interestingly, it was shown that the mutated $EF_2$ has similar binding mechanism as $EF_1$, namely, the N-terminal part of the loop are coordinated to $Ca^{2+}$ earlier than the C-terminal ligands.[45] These results suggest that the charged state of the residues to which $Ca^{2+}$ is coordinated plays a crucial role in the mechanism of $Ca^{2+}$ binding and allostery.[22]

The cCaM has the similar $Ca^{2+}$ binding order except that the binding orders of the $EF_3$ and $EF_4$ in the cCaM correspond to those of the $EF_2$ and $EF_1$ in the nCaM (see Supplementary Fig.S4 online), as expected from the similarity of the sequences of the respective $Ca^{2+}$ loops. As shown in Fig. 1 and Fig.S1 (see Supplementary Fig.S1 online), the residue at the $l5$ position of the $EF_1$ ($EF_4$) in the nCaM (cCaM) is charged, whereas that of the $EF_2$ ($EF_3$) in the nCaM (cCaM) is neutral.

## $Ca^{2+}$ binding-induced rotation of EF-hand helices

Structures of nCaM show that there are several hydrophobic residues located around Ile27 and Ile63 whose non-polar side-chains stack against each other to form the center of the hydrophobic core[52,54] (Fig. 5D). During the $Ca^{2+}$ binding and conformational transition, the hydrophobic cluster formed by these residues, including Phe16, Phe19, Ile27, Leu32, Val35, Ile52, Val55, Ile63 and Phe68, are almost rigid (see Supplementary Fig.S5 online). Comparison of the structures in the apo- and holo- states suggests that the two helices of the EF-hand rotate around the hydrophobic cluster during the conformational transition.

To demonstrate the coupling between the $Ca^{2+}$ binding and the EF-hand opening, we

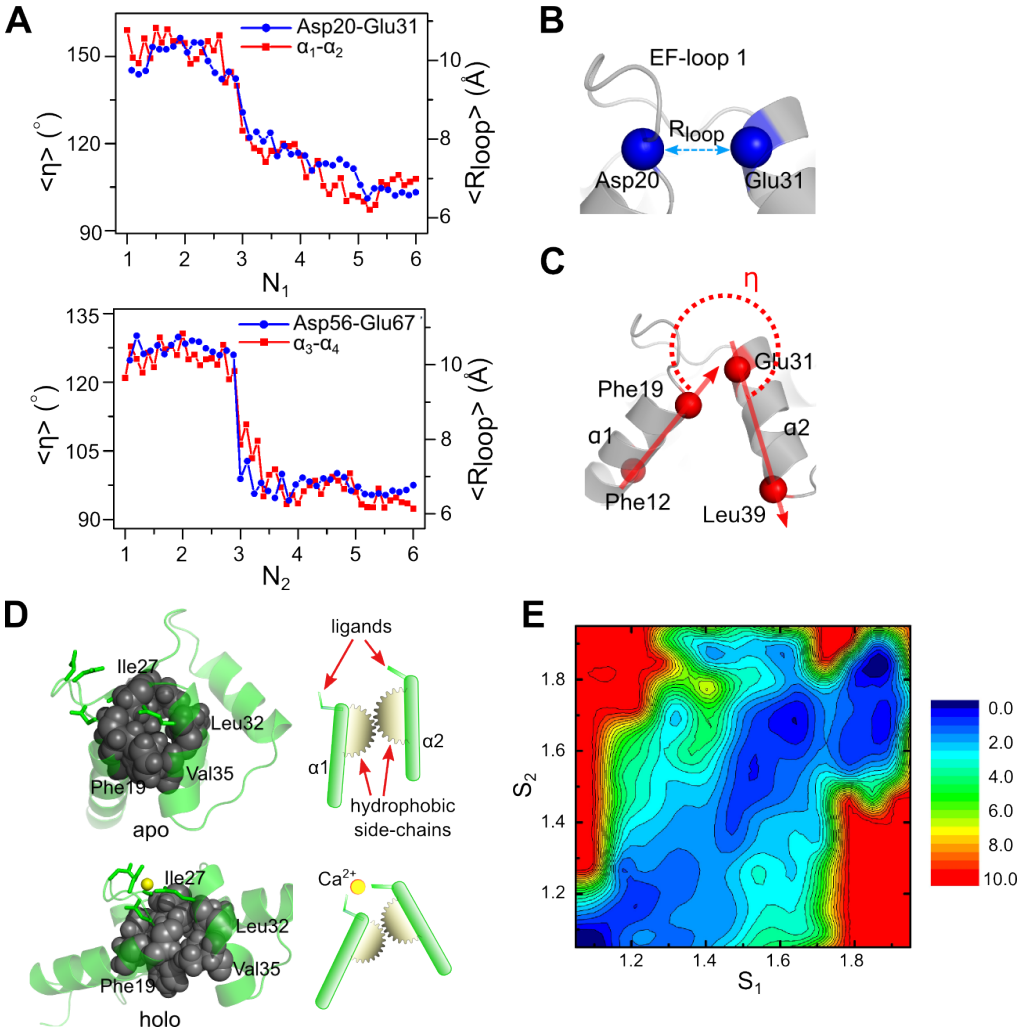


Figure 5: $Ca^{2+}$ binding induced rotation of EF-hand helices. (A) The distance between close ends of EF-loop 1 (represented by the $C_\alpha$ atoms from Asp20 and Glu31) and inter-helical angle between the helices in $EF_1$ as a function of $N_1$ (upper panel). The same results for the $EF_2$ are shown in the lower panel of (A). (B) Schematic diagram illustrating the end-end distance of EF-loop1 and (C) the inter-helical angles of $EF_1$. The end-end distance of EF-loop is represented by the distance between $C_\alpha$ atoms: EF-loop1 by Asp20–Glu31, and EF-loop2 by Asp56–Glu67. The direction of helices are represented by vectors pointing from one residue's $C_\alpha$ atom to another residue's $C_\alpha$ atom: $\alpha 1$ by Phe12–Phe19, $\alpha 2$ by Glu31–Leu39, $\alpha 3$ by Leu48–Val55, and $\alpha 4$ by Phe68–Lys75. (D) Schematic diagram of the $Ca^{2+}$ binding induced EF-hand helix rotation. Black spheres indicate the hydrophobic core in $EF_1$. (E) Free energy profile of nCaM conformational transition projected onto $S_1$ and $S_2$. The free energy scale is in kcal/mol, and the isolines are drawn using a spacing of 0.5kcal/mol.

calculated the distance between the EF-loop ends ($R_{loop}$, is the distance between the blue residues in Fig. 5B) and the inter-helical angles between the helices ($\eta$, denoted by the red arrows in Fig. 5C, which are represented by vectors pointing from one residue's $C_\alpha$ to another) of the two EF-hands, respectively. The results in Fig. 5A show that $R_{loop}$ decreases upon $Ca^{2+}$ binding, thus pulling the ends of the EF-hand helices close together (blue lines). In particular, binding of the third ligand to $Ca^{2+}$, which corresponds to the binding of the terminal residues of the EF-hand loops to the $Ca^{2+}$ by direct interactions in $EF_2$ or by water bridged interactions in $EF_1$, has the most prominent effect in changing the distance between the two close ends. Meanwhile, the angles between the two helices increase (red lines), indicating the rotation of the EF-hand helices. During the rotation, the hydrophobic cluster, which is stable during the $Ca^{2+}$ binding, acts as the pivot (Fig. 5D). Furthermore, the rotation of the EF-hand helices is accompanied by the reconfiguration of the surrounding hydrogen bonds (see Supplementary Fig.S5D, E online). Taken together these results demonstrate that the rotation of the EF-hand helices is coupled to $Ca^{2+}$ binding, which is consistent with the free energy landscapes shown in Fig. 2. $Ca^{2+}$ binding induced rotation of the EF-hand helices was also noted in other simulation work.[61]

The large conformational rearrangement between the two helices of the $EF_1$ with the coordination of the third ligand is somewhat surprising since the conformational restraint to the inter-helix orientation imposed by the coordination of the Asp24 is limited, as envisaged from the coordination structure of the holo conformation (Fig. 1). One possible origin for the observed large-amplitude rotation is the tight coupling between the two EF-hands. As shown in Fig. 5E, the conformational changes of the two EF-hands mostly follow the diagonal line of the two dimensional free energy landscape, which may suggest the tight coupling and cooperativity between the two EF-hands. Consequently, the coordination of the terminal residues of the EF-hand loop to the $Ca^{2+}$ in $EF_2$ leads to the conformational transition of $EF_2$ from closed to open conformations due to the strong geometric restraint, which then induces the partial opening of the $EF_1$ helices. In fact, the tight coupling between the two

EF-hands in both nCaM and cCaM have been observed in experiments,[25,37] which is in line with the above discussions.

## Bridging water molecules lower the free energy barrier between the allosteric states

As mentioned above, water-bridged interactions play a crucial role during $Ca^{2+}$ binding, and hence in the allosteric transitions in CaM. To further demonstrate the role of water molecules, we performed detailed analysis of the ensemble of conformations containing water-bridged coordinated structures. We assume that a water-bridged coordination is formed if the following conditions are satisfied: (i) the distance from oxygen of water molecule ($O_w$) to $Ca^{2+}$ is less than 2.8Å; and (ii) the hydrogen bond is formed between water and the native ligand. We note that for each residue listed in Table 1, the $Ca^{2+}$-water-native ligand conformation exists in certain stages of the binding process with high probability. These results suggest that before the final chelation process, the native ligands already develop indirect interactions with $Ca^{2+}$ bridged by water molecules. For example, after binding of $Ca^{2+}$ to five of the native ligands of $EF_2$, the last native ligand, Thr62, is not "free", but has a probability of 0.83 to be bridged to the $Ca^{2+}$ by a water molecule (Table 1).

To quantitatively evaluate the contribution of water molecules to the $Ca^{2+}$ binding process, we characterize the water bridged binding of the Glu31 to the $Ca^{2+}$ in the final step of the $Ca^{2+}$ binding to the $EF_1$. We used well-tempered metadynamics to extract the free energy profile along the collective variable $D$, which is defined as the distance between $Ca^{2+}$ and the closest side-chain oxygen of Glu31 (see **Methods** section). As a control, we also designed a system in which the electrostatic interactions between the bridging water molecule and Glu31 side-chain atoms were turned off. The differences between the two simulations reflect the net effect of the bridging water on the binding free energy landscape. When the interaction of the bridging water includes the electrostatic potential, an intermediate is present in the free energy profile at $D \approx 4.3$Å (see Fig. 6A, black line), in which the Glu31

is bridged to the $Ca^{2+}$ by the bridging water molecule (Fig. 6B). Note that the height of free energy barrier is comparable with the value of the free energy barrier between $N_\alpha = 4$ and $N_\alpha = 5$, as shown in Fig. 2A. In contrast, when the electrostatic interactions involving the bridging water molecule are switched off, a high free energy barrier is observed ($\sim$ 6kcal/mol, shown in Fig. 6A, red line). We surmise that water reduces the free energy barrier by bridging the $Ca^{2+}$–Glu31 interaction, therefore speeding up the coordination between the $Ca^{2+}$ and Glu31.

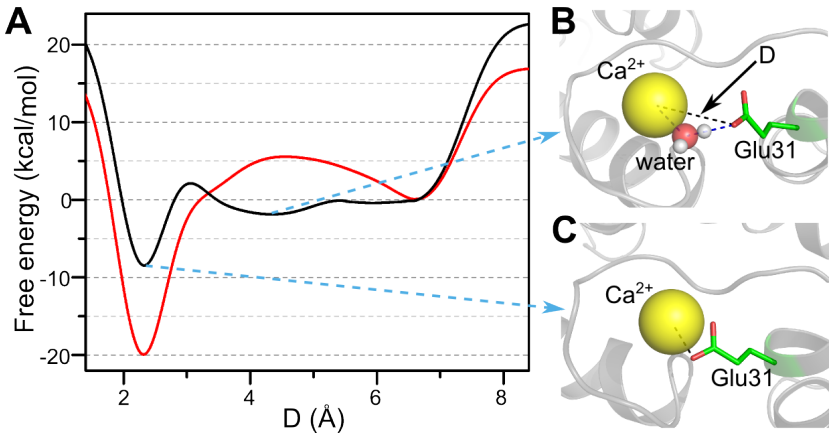


Figure 6: Free energy profiles of water bridged coordination of Glu31 side-chain oxygen atoms to the $Ca^{2+}$. (A) Potential of mean force for the binding/unbinding process of Glu31 to $Ca^{2+}$ as a function of the minimum distance between side-chain oxygen atoms of Glu31 and $Ca^{2+}$. The black line illustrates the results with the water molecules being realistically treated. The red line shows the results with electrostatic interactions involving the bridging water molecules being turned off. (B) The water-bridged coordination of Glu31 oxygen and $Ca^{2+}$, where $D = 4.3$Å is a local free energy minimum. (C) shows the direct coordination bond of Glu31 oxygen and the $Ca^{2+}$, which corresponds to the most stable state at $D = 2.3$Å.

Two possible effects may contribute to the reduction of the free energy barrier by the bridging water. First, the attractive interaction due to the bridging waters tends to decrease the free energy barrier. Second, the bridging water reduces the translational entropy of the captured $Ca^{2+}$, therefore decreasing the entropy penalty during the $Ca^{2+}$–Glu31 coordination, which can also contribute to the reduction of the free energy barrier. We propose that this kind of contribution of water molecule to the binding of metal ions should be a common feature in other metal-ion induced biological processes.

Table 1: Probabilities of non-native ligand coordination and water-bridged native ligand coordination. $O_w$ refers to oxygen in water. $N_\alpha$ is the number of coordinated native ligands.

| $EF_1$ | $N_1$=3 | $N_1$=4 | $N_1$=5 |
|---|---|---|---|
| $Ca^{2+}$–$O_w$–Thr26 | 0.42 | 0.03 | 0 |
| $Ca^{2+}$–$O_w$–Glu31 | 0.23 | 0.67 | 0.02 |
| $EF_2$ | $N_2$=3 | $N_2$=4 | $N_2$=5 |
| $Ca^{2+}$–$O_w$–Asn60 | 0.17 | 0.27 | 0 |
| $Ca^{2+}$–$O_w$–Thr62 | 0.49 | 0.52 | 0.83 |
| $Ca^{2+}$–Asp64 | 0.52 | 0 | 0 |

# Conclusion

Allosteric transitions are ubiquitous in biology. Nowhere it is more prominent in modulating large conformational changes over long distances (nearly 20Å) than it is in CaM induced by $Ca^{2+}$ binding. Using all-atom molecular dynamics simulations in conjunction with metadynamics, which enables efficient sampling of the conformational space, we have established that in the $Ca^{2+}$ binding coupled allosteric transition water plays a crucial role. The high free energy cost dehydration of $Ca^{2+}$ occurs in steps with the number of waters lost at different stages being compensated by gain in chelation to the charged residues in the loops of the EF-hands. The overall picture that emerges is that there is a coordinated interplay between ligand binding, loss of water around the cation, and subsequent changes in the conformations of the enzyme. We propose that similar mechanisms, with water playing an important role, might also mediate allosteric transitions in molecular machines, such as molecular chaperones, molecular motors and cell adhesion molecules, in which allosteric transitions are often triggered by cations. Our results also demonstrated that there is an asymmetry in the $Ca^{2+}$ and conformational transitions in the EF-hand pair of isolated CaM domains despite the overall structural similarity. The $Ca^{2+}$-coupled closed to open transitions in the two hands occur by an entirely different mechanism, which could facilitate the differing functional requirements of CaM.

In our metadynamics simulations, for better convergence, we prevent $Ca^{2+}$ ions from leaving too far from the binding sites by applying a lower limit to the coordination number,

one of the reaction coordinates. Such a restraint may introduce bias to the calculated conformational distributions around the apo state, which makes quantitative discussions impossible. Future studies without applying such restraint would be useful in discussing the molecular mechanism of the $Ca^{2+}$ capturing during the early stage of the $Ca^{2+}$ binding event. In addition, including the downstream binding partners of the CaM in such simulations would also be important to fully understand the propagation of allosteric signal in a molecular level.

# Methods

We used the NMR structure of *Xenopus* nCaM for the holo form with 1J7O[54] as the Protein Data Bank (PDB) entry. The apo form with the same sequence (residue 1 to 76) was taken from the NMR structure of *X. laevis* CaM with PDB code 1CFD.[52] All MD simulations were carried out using GROMACS 4.5.5[62] with the OPLS/AA force field.[63] The $Ca^{2+}$-nCaM system was solvated in the SPC/E water box together with $K^+$ and $Cl^-$ ions to mimic the ion concentration of $0.15M$. The whole system had 17,278 atoms, of which 16,086 atoms were from water. We used the periodic boundary condition where the size of unit box is $\sim 62.8 \times 62.8 \times 44.2$ Å$^3$. Energy minimization was performed before the MD simulations. Before running metadynamics simulations the $Ca^{2+}$-nCaM systems were heated to 300K in the NVT ensemble and then equilibrated for 10 ns MD under NPT conditions, with $P = 1$atm and $T = 300$K. Periodic conditions were used and electrostatic interactions were calculated using the particle-mesh Ewald algorithm. The simulations for the cCaM were conduced similarly.

## Collective Variables (CVs) in metadynamics

We used the "bias-exchange"[46] form and "well-tempered"[50] algorithm of metadynamics to accelerate conformational sampling, using the PLUMED 1.3 package.[64] The CVs used to study the $Ca^{2+}$-binding coupled conformational change of CaM were chosen to describe

the rate-limiting events involving the binding of $Ca^{2+}$ and the subsequent conformational transition of the protein.

The events driving the closed to open transition involve movement of a number of particles from distant parts of CaM domains. In order to capture such an allosteric movement, we need suitable reaction coordinates. Since the major events in the closed $\rightarrow$ open transition are triggered by $Ca^{2+}$ binding, we constructed CV involving the oxygen atoms (ligands) of the residues in the holo structure that are coordinated to $Ca^{2+}$. In terms of these native ligands, we define the collective variables, $N_\alpha$ ($\alpha = 1$ and 2 (3 and 4) for $EF_1$ and $EF_2$ ($EF_3$ and $EF_4$), respectively, of the nCaM and cCaM) to describe the number of native ligands that are coordinated to $Ca^{2+}$:

$$N_\alpha = \sum_{i \in \text{native ligands}} k_i^\alpha, \tag{1}$$

where $k_i^\alpha$ is defined using the switching function,

$$k_i^\alpha = \begin{cases} 1 & \text{for } r_i^\alpha \leq d_0 \\ \dfrac{1-\left(\frac{r_i^\alpha - d_0}{r_0^\alpha}\right)^4}{1-\left(\frac{r_i^\alpha - d_0}{r_0^\alpha}\right)^6} & \text{for } r_i^\alpha > d_0 \end{cases} \tag{2}$$

In equation (2), $r_i^\alpha$ is the distance from the $i^{th}$ native ligand to the $\alpha^{th}$ $Ca^{2+}$. By native ligand we mean the oxygen atoms from distinct amino acids that are linked to $Ca^{2+}$ and are present in the native (NMR) holo structure. We chose $d_0 = 2.5$Å and $r_0 = 0.3$Å. For all the Asp residues, the two oxygens from the same residue were considered "degenerate", namely, when more than one oxygen is coordinated to $Ca^{2+}$, we consider only one of them to be a native ligand. However, for the Glu residues in the $12^{th}$ position of the EF-loops of nCaM and cCaM, two oxygens are treated as individual ligands. We treated coordination of $Ca^{2+}$ to Asp differently from binding to Glu because in the holo structure of the nCaM and cCaM (PDB entry 1J7O and 1J7P, respectively) $Ca^{2+}$ is coordinated to both oxygen atoms of Glu

but only to one of the Asp oxygen atoms.

We also used the "path collective variables" calculated using,

$$S_\alpha = \frac{\sum_{i=1}^{2} i e^{-\lambda d(X_i^\alpha, X(t))}}{\sum_{i=1}^{2} e^{-\lambda d(X_i^\alpha, X(t))}}, \tag{3}$$

where $\alpha = 1, 2, 3,$ and 4 dictates the $\alpha^{th}$ EF-hand, and $d(X_i^\alpha, X(t))$ is the mean square deviation from the closed ($i = 1$) and open ($i = 2$) structure for a given conformation $X(t)$. A small value of $S_\alpha$ corresponds to closed structure and a large value of $S_\alpha$ corresponds to open structure. We used $\lambda = 10$ in our simulations.

To use the bias-exchange method with metadynamics, we designed 5 replicas. In the first replica, there is no bias in the CVs. In each of the other four replicas, a bias was applied to one of CVs, including $N_1$, $N_2$, $S_1$, and $S_2$ for the nCaM simulations, and $N_3$,$N_4$, $S_3$, and $S_4$ for the cCaM simulations. Exchange between replicas was attempted every 10,000 MD steps, and each replica lasts for 250ns. In the well-tempered algorithm, we used a bias factor of 30 for the rescaling of the Gaussian height, and 0.2kJ/mol as the initial Gaussian height. To get better convergence of the simulations, lower boundaries of the $N_1$, $N_2$, $N_3$ and $N_4$ were set at 0.5 (for all the 5 replicas), which prevents the $Ca^{2+}$ from departing too far from the binding sites. More detailed descriptions of the simulation procedure can be found in Supplementary Methods and Supplementary Fig.S6, S7 and S8 online.

## Coordination probability

Binding pathways are quantified using the probability, $P(i, \overline{N_\alpha})$, that the $i^{th}$ residue is coordinated to $Ca^{2+}$ when the total ligand number of EF-hand $\alpha$ is $\overline{N_\alpha}$ ($\overline{N_\alpha} = 1, 2, \ldots, 6$). We define $P(i, \overline{N_\alpha})$ using

$$P(i, \overline{N_\alpha}) = \frac{\int k_i^\alpha P(k_i^\alpha, N_\alpha) \theta_{\overline{N_\alpha}}(N_\alpha)\, \mathrm{d}k_i^\alpha\, \mathrm{d}N_\alpha}{\int P(k_i^\alpha, N_\alpha) \theta_{\overline{N_\alpha}}(N_\alpha)\, \mathrm{d}k_i^\alpha\, \mathrm{d}N_\alpha}, \tag{4}$$

where $N_\alpha$ and $k_i^\alpha$ are defined in equation (1) and equation (2), and $\theta_{\overline{N_\alpha}}(N_\alpha)$ is a step function:

$$\theta_{\overline{N_\alpha}}(N_\alpha) = \begin{cases} 1 & \text{for } N_\alpha \in [\overline{N_\alpha} - 0.5, \overline{N_\alpha} + 0.5) \\ 0 & \text{for } N_\alpha \notin [\overline{N_\alpha} - 0.5, \overline{N_\alpha} + 0.5) \end{cases} \tag{5}$$

$P(k_i^\alpha, N_\alpha)$ is a two dimensional probability distribution of the variables $k_i^\alpha$ and $N_\alpha$, which cannot be directly calculated as the average over time from the metadynamics. We use the reweighting techniques described in Ref.[51] to reconstruct the unbiased distribution. We calculated the two-dimensional probability distributions on a $60 \times 60$ grid. Then we constructed bins on the $N_\alpha$ dimension as $(0, 0.5), [0.5, 1.5), [1.5, 2.5), \ldots, [4.5, 5.5), [5.5, 6]$, and binned any $N_\alpha \in [\overline{N_\alpha} - 0.5, \overline{N_\alpha} + 0.5)$ into integer values $\overline{N_\alpha}$.

The occurrence probability of the water-bridged coordination has the same form as equation (4), except for the definition of $k_i$. For the water-bridged coordination, $k_i = 1$ when the oxygen of water is within 2.8Å of the $Ca^{2+}$ and at the same time within 3.5Å of the oxygens from a native liganding residue, and is zero otherwise.

## Water-bridged coordination of Glu31 to the $Ca^{2+}$

We also used well-tempered metadynamics to study water-bridged coordination of Glu31 to the $Ca^{2+}$ for the nCaM. The minimum distance between the $Ca^{2+}$ and two oxygen atoms of Glu31 is chosen as the collective variable $D$,[64] which we define as:

$$D = \frac{\sigma}{\ln \sum_i \exp(\sigma / \|r_i\|)}, \tag{6}$$

where $r_i$ $(i = 1, 2)$ is the distance between each oxygen and the $Ca^{2+}$, and $\sigma = 5000$Å. The well-tempered rescaling factor is 12, and the initial Gaussian height is 0.2kJ/mol.

In the control simulation, once a water molecule comes into the first ligand shell of $Ca^{2+}$ and simultaneously within 3.5Å distance of any of the two oxygen atoms of Glu31, the electrostatic interactions between the water and the side-chain heavy atoms of Glu31 are

turned off. This was accomplished by modifying the source code of GROMACS package.

To achieve better convergence we use a restraining potential at $D = 6.5$Å to limit the region of the phase space accessible during the simulation:

$$V_{wall}(D) = K(D - D_{wall})^2, \text{for D} > 6.5 \text{ Å}, \tag{7}$$

where $K = 50kcal/mol/\text{Å}^2$ and $D_{wall} = 6.5$Å. We performed 20 independent 100ns simulations for each system, and then calculated the ensemble average to obtain the free energy reported in Fig. 6. Comparison of the simulations with and without electrostatic interactions allows us to assess the role water plays in modulating the binding of $Ca^{2+}$.

## Acknowledgement

**Acknowledgments:** This work was supported by the 973 program (2013CB834104), and the NNSF of China (11574132 and 11334004). Part of this work was done while DT was a visiting Professor in Nanjing University. DT acknowledges the NSF (CHE09–14033) for partial support of this work. The numerical calculations in this paper have been done on the IBM Blade cluster system in the High Performance Computing Center of Nanjing University.

## Supporting Information Available

Additional details describing the MD simulation, analysis of the simulation data, and miscellaneous derivations are provided in Supporting Information and Supporting Figures S1–S8.

## References and Notes

(1) Clapham, D. E. Calcium Signaling. *Cell* **2007**, *131*, 1047–1058.

(2) Osawa, M.; Tokumitsu, H.; Swindells, M. B.; Kurihara, H.; Orita, M.; Shibanuma, T.;

Furuya, T.; Ikura, M. A Novel Target Recognition Revealed by Calmodulin in Complex with Ca2+-Calmodulin-Dependent Kinase Kinase. *Nature Struct. Biol.* **1999**, *6*, 819–824.

(3) Walsh, M. P. Calmodulin and the Regulation of Smooth Muscle Contraction. *Mol. Cell. Biochem.* **1994**, *135*, 21–41.

(4) Means, A. R. Calcium, Calmodulin and Cell Cycle Regulation. *FEBS Lett.* **1994**, *347*, 1–4.

(5) Gunther, N.; Chris, B.; Rainer, K.; Nam-Hai, C. Calcium/Calmodulin-Dependent and -Independent Phytochrome Signal Transduction Pathways. *Cell* **1993**, *73*, 937–952.

(6) Jiang, X.; Li, J.; Paskind, M.; Epstein, P. M. Inhibition of Calmodulin-Dependent Phosphodiesterase Induces Apoptosis in Human Leukemic Cells. *Proc. Natl. Acad. Sci. U.S.A.* **1996**, *93*, 11236–11241.

(7) Barbato, G.; Ikura, M.; Kay, L. E.; Pastor, R. W.; Bax, A. Backbone Dynamics of Calmodulin Studied by Nitrogen-15 Relaxation using Inverse Detected Two-Dimensional NMR Spectroscopy: The Central Helix is Flexible. *Biochemistry* **1992**, *31*, 5269–5278.

(8) Fiorin, G.; Biekofsky, R. R.; Pastore, A.; Carloni, P. Unwinding the Helical Linker of Calcium-Loaded Calmodulin: A Molecular Dynamics Study. *Proteins* **2005**, *61*, 829–839.

(9) Gifford, J. L.; Walsh, M. P.; Vogel, H. J. Structures and Metal-Ion-Binding Properties of the $Ca^{2+}$-Binding Helix-Loop-Helix EF-Hand Motifs. *Biochem. J.* **2007**, *405*, 199–221.

(10) Lewit-Bentley, A.; Réty, S. EF-Hand Calcium-Binding Proteins. *Curr. Opin. Struct. Biol.* **2000**, *10*, 637–643.

(11) Grabarek, Z. Structural Basis for Diversity of the EF-Hand Calcium-Binding Proteins. *J. Mol. Biol.* **2006**, *359*, 509–525.

(12) Nelson, M. R.; Chazin, W. J. Structures of EF-hand Ca(2+)-Binding Proteins: Diversity in the Organization, Packing and Response to Ca2+ Binding. *Biometals* **1998**, *11*, 297–318.

(13) Tsai, C. J.; Kumar, S.; Ma, B.; Nussinov, R. Folding Funnels, Binding Funnels, and Protein Function. *Protein Sci.* **1999**, *8*, 1181–1190.

(14) Swain, J. F.; Gierasch, L. M. The Changing Landscape of Protein Allostery. *Curr. Opin. Struct. Biol.* **2006**, *16*, 102–108.

(15) Hyeon, C.; Lorimer, G. H.; Thirumalai, D. Dynamics of Allosteric Transitions in GroEL. *Proc. Natl. Acad. Sci. U.S.A.* **2006**, *103*, 18939–18944.

(16) Koga, F.; Xu, W.; Karpova, T. S.; McNally, J. G.; Baron, R.; Neckers, L. Hsp90 Inhibition Transiently Activates Src Kinase and Promotes Src-Dependent Akt and Erk Activation. *Proc. Natl. Acad. Sci. U.S.A.* **2006**, *103*, 11318–11322.

(17) Weinkam, P.; Pons, J.; Sali, A. Structure-Based Model of Allostery Predicts Coupling between Distant Sites. *Proc. Natl. Acad. Sci. U.S.A.* **2012**, *109*, 4875–4880.

(18) Zheng, W.; Brooks, B. R.; Thirumalai, D. Low-Frequency Normal Modes that Describe Allosteric Transitions in Biological Nanomachines are Robust to Sequence Variations. *Proc. Natl. Acad. Sci. U.S.A.* **2006**, *103*, 7664–7669.

(19) Li, W.; Wolynes, P. G.; Takada, S. Frustration, Specific Sequence Dependence, and Nonlinearity in Large-Amplitude Fluctuations of Allosteric Proteins. *Proc. Natl. Acad. Sci. U.S.A.* **2011**, *108*, 3504–3509.

(20) Ferreiro, D. U.; Hegler, J. A.; Komives, E. A.; Wolynes, P. G. On the Role of Frustration

in the Energy Landscapes of Allosteric Proteins. *Proc. Natl. Acad. Sci. U.S.A.* **2011**, *108*, 3499–3503.

(21) Winkler, W. C.; Breaker, R. R. Regulation of Bacterial Gene Expression by Riboswitches. *Annu. Rev. Microbiol.* **2005**, *59*, 487–517.

(22) Csermely, P.; Palotai, R.; Nussinov, R. Induced Fit, Conformational Selection and Independent Dynamic Segments: An Extended View of Binding Events. *Trends Biochem. Sci.* **2010**, *35*, 539–546.

(23) Grant, B. J.; Gorfe, A. A.; McCammon, J. A. Large Conformational Changes in Proteins: Signaling and other Functions. *Curr. Opin. Struct. Biol.* **2010**, *20*, 142–147.

(24) Li, W.; Wang, W.; Takada, S. Energy Landscape Views for Interplays among Folding, Binding, and Allostery of Calmodulin Domains. *Proc. Natl. Acad. Sci. U.S.A.* **2014**, *111*, 10550–10555.

(25) Linse, S.; Helmersson, a.; Forsén, S. Calcium Binding to Calmodulin and its Globular Domains. *J. Biol. Chem.* **1991**, *266*, 8050–8054.

(26) Barton, N. P.; Verma, C. S.; Caves, L. S. D. Inherent Flexibility of Calmodulin Domains: A Normal-Mode Analysis Study. *J. Phys. Chem. B* **2002**, *106*, 11036–11040.

(27) Junker, J. P.; Ziegler, F.; Rief, M. Ligand-Dependent Equilibrium Fluctuations of Single Calmodulin Molecules. *Science* **2009**, *323*, 633–637.

(28) Chen, Y.-G.; Hummer, G. Slow Conformational Dynamics and Unfolding of the Calmodulin C-Terminal Domain. *J. Am. Chem. Soc.* **2007**, *129*, 2414–2415.

(29) Price, E. S.; Aleksiejew, M.; Johnson, C. K. FRET-FCS Detection of Intralobe Dynamics in Calmodulin. *J. Phys. Chem. B* **2011**, *115*, 9320–9326.

(30) Tripathi, S.; Portman, J. J. Inherent Flexibility Determines the Transition Mechanisms of the EF-Hands of Calmodulin. *Proc. Natl. Acad. Sci. U.S.A.* **2009**, *106*, 2104–2109.

(31) Itoh, K.; Sasai, M. Statistical Mechanics of Protein Allostery: Roles of Backbone and Side-Chain Structural Fluctuations. *J. Chem. Phys.* **2011**, *134*, 125102.

(32) Ovchinnikov, V.; Karplus, M. Analysis and Elimination of a Bias in Targeted Molecular Dynamics Simulations of Conformational Transitions: Application to Calmodulin. *J. Phys. Chem. B* **2012**, *116*, 8584–8603.

(33) Li, W.; Wang, J.; Zhang, J.; Wang, W. Molecular Simulations of Metal-Coupled Protein Folding. *Current Opinion in Structural Biology* **2015**, *30*, 25–31.

(34) Evenäs, J.; Malmendal, A.; Thulin, E.; Carlström, G.; Forsén, S. $Ca^{2+}$ Binding and Conformational Changes in a Calmodulin Domain. *Biochemistry* **1998**, *37*, 13744–13754.

(35) Martin, S. R.; Maune, J. F.; Beckingham, K.; Bayley, P. M. Stopped-Flow Studies of Calcium Dissociation from Calcium-Binding-Site Mutants of Drosophila Melanogaster Calmodulin. *Eur. J. Biochem.* **1992**, *205*, 1107–1114.

(36) Park, H. Y.; Kim, S. A.; Korlach, J.; Rhoades, E.; Kwok, L. W.; Zipfel, W. R.; Waxham, M. N.; Webb, W. W.; Pollack, L. Conformational Changes of Calmodulin upon $Ca^{2+}$ Binding Studied with a Microfluidic Mixer. *Proc. Natl. Acad. Sci. U.S.A.* **2008**, *105*, 542–547.

(37) Malmendal, a.; Evenäs, J.; Forsén, S.; Akke, M. Structural Dynamics in the C-Terminal Domain of Calmodulin at Low Calcium Levels. *J. Mol. Biol.* **1999**, *293*, 883–899.

(38) Evenäs, J.; Malmendal, A.; Akke, M. Dynamics of the Transition between Open and Closed Conformations in a Calmodulin C-Terminal Domain Mutant. *Structure* **2001**, *9*, 185–195.

(39) Ohashi, W.; Hirota, H.; Yamazaki, T. Solution Structure and Fluctuation of the

Mg(2+)-Bound form of Calmodulin C-Terminal Domain. *Protein Sci.* **2011**, *20*, 690–701.

(40) Meyer, D. F.; Mabuchi, Y.; Grabarek, Z. The Role of Phe-92 in the Ca(2+)-Induced Conformational Transition in the C-Terminal Domain of Calmodulin. *J. Biol. Chem.* **1996**, *271*, 11284–11290.

(41) Xiong, L.-W.; Kleerekoper, Q. K.; Wang, X.; Putkey, J. a. Intra- and Interdomain Effects due to Mutation of Calcium-Binding Sites in Calmodulin. *J. Biol. Chem.* **2010**, *285*, 8094–8103.

(42) Evenäs, J.; Thulin, E.; Malmendal, a.; Forsén, S.; Carlström, G. NMR Studies of the E140Q Mutant of the Carboxy-Terminal Domain of Calmodulin Reveal Global Conformational Exchange in the Ca2+-Saturated State. *Biochemistry* **1997**, *36*, 3448–3457.

(43) Zhang, Y.; Tan, H.; Lu, Y.; Jia, Z.; Chen, G. Ca(2+) Dissociation from the C-Terminal EF-Hand Pair in Calmodulin: A Steered Molecular Dynamics Study. *FEBS letters* **2008**, *582*, 1355–1361.

(44) Kukic, P.; Lundstrom, P.; Camiloni, C.; Johan, E.; Mikael, A.; Vendruscolo, M. Structural Insights into the Calcium-Mediated Allosteric Transition in the C-Terminal Domain of Calmodulin from Nuclear Magnetic Resonance Measurements. *Biochemistry* **2016**, 10.1021/acs.biochem.5b00961.

(45) Grabarek, Z. Structure of a Trapped Intermediate of Calmodulin: Calcium Regulation of EF-Hand Proteins from a New Perspective. *J. Mol. Biol.* **2005**, *346*, 1351–1366.

(46) Piana, S.; Laio, A. A Bias-Exchange Approach to Protein Folding. *J. Phys. Chem. B* **2007**, *111*, 4553–4559.

(47) Komeiji, Y.; Ueno, Y.; Uebayasi, M. Molecular Dynamics Simulations Revealed $Ca^{2+}$-Dependent Conformational Change of Calmodulin. *FEBS Lett.* **2002**, *521*, 133–139.

(48) Likić, V. A.; Strehler, E. E.; Gooley, P. R. Dynamics of $Ca^{2+}$-Saturated Calmodulin D129N Mutant Studied by Multiple Molecular Dynamics Simulations. *Protein Sci.* **2003**, *12*, 2215–2229.

(49) Zhang, B. W.; Jasnow, D.; Zuckerman, D. M. Efficient and Verified Simulation of a Path Ensemble for Conformational Change in a United-Residue Model of Calmodulin. *Proc. Natl. Acad. Sci. U.S.A.* **2007**, *104*, 18043–18048.

(50) Barducci, A.; Bussi, G.; Parrinello, M. Well-Tempered Metadynamics: A Smoothly Converging and Tunable Free-Energy Method. *Phys. Rev. Lett.* **2008**, *100*, 020603.

(51) Bonomi, M.; Barducci, A.; Parrinello, M. Reconstructing the Equilibrium Boltzmann Distribution from Well-Tempered Metadynamics. *J. Comp. Chem.* **2009**, *30*, 1615–1621.

(52) Chou, J. J.; Li, S.; Klee, C. B.; Bax, A. Solution Structure of $Ca^{2+}$-Calmodulin Reveals Flexible Hand-Like Properties of its Domains. *Nature Struct. Biol.* **2001**, *8*, 990–997.

(53) Vigil, D.; Gallagher, S. C.; Trewhella, J.; García, A. E. Functional Dynamics of the Hydrophobic Cleft in the N-Domain of Calmodulin. *Biophys. J.* **2001**, *80*, 2082–2092.

(54) Kuboniwa, H.; Tjandra, N.; Grzesiek, S.; Ren, H.; Klee, C. B.; Bax, A. Solution Structure of Calcium-Free Calmodulin. *Nature Struct. Biol.* **1995**, *2*, 768–776.

(55) Wilson, C. J.; Apiyo, D.; Wittung-Stafshede, P. Role of Cofactors in Metalloprotein Folding. *Q. Rev. Biophys.* **2004**, *37*, 285–314.

(56) Li, W.; Zhang, J.; Wang, J.; Wang, W. Metal-Coupled Folding of Cys2His2 Zinc-Finger. *J. Am. Chem. Soc.* **2008**, *130*, 892–900.

(57) Lee, Y.-M.; Lim, C. Factors Controlling the Reactivity of Zinc Finger Cores. *J. Am. Chem. Soc.* **2011**, *133*, 8691–8703.

(58) Kobayashi, C.; Takada, S. Protein Grabs a Ligand by Extending Anchor Residues: Molecular Simulation for $Ca^{2+}$ Binding to Calmodulin Loop. *Biophys. J.* **2006**, *90*, 3043–3051.

(59) Pavlov, M.; Siegbahn, P. E. M.; Sandström, M. Hydration of Beryllium, Magnesium, Calcium, and Zinc Ions using Density Functional Theory. *J. Phys. Chem. A* **1998**, *102*, 219–228.

(60) Jalilehvand, F.; Spå ngberg, D.; Lindqvist-Reis, P.; Hermansson, K.; Persson, I.; Sandström, M. Hydration of the Calcium Ion. An EXAFS, Large-Angle X-Ray Scattering, and Molecular Dynamics Simulation Study. *J. Am. Chem. Soc.* **2001**, *123*, 431–441.

(61) Goto, K.; Toyama, A.; Takeuchi, H.; Takayama, K.; Saito, T.; Iwamoto, M.; Yeh, J. Z.; Narahashi, T. $Ca^{2+}$ Binding Sites in Calmodulin and Troponin C Alter Interhelical Angle Movements. *FEBS Lett.* **2004**, *561*, 51–57.

(62) Hess, B.; Kutzner, C.; van der Spoel, D.; Lindahl, E. GROMACS 4: Algorithms for Highly Efficient, Load-Balanced, and Scalable Molecular Simulation. *J. Chem. Theor. Comp.* **2008**, *4*, 435–447.

(63) Kaminski, G. A.; Friesner, R. A.; Tirado-Rives, J.; Jorgensen, W. L. Evaluation and Reparametrization of the OPLS-AA Force Field for Proteins via Comparison with Accurate Quantum Chemical Calculations on Peptides. *J. Phys. Chem. B* **2001**, *105*, 6474–6487.

(64) Bonomi, M.; Branduardi, D.; Bussi, G.; Camilloni, C.; Provasi, D.; Raiteri, P.; Donadio, D.; Marinelli, F.; Pietrucci, F.; Broglia, R. A.; Parrinello, M. PLUMED: A Portable Plugin for Free-Energy Calculations with Molecular Dynamics. *ChemPhysChem* **2009**, *180*, 1961–1972.
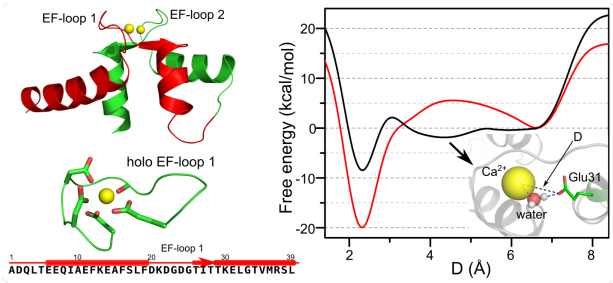
# Table of Contents graphic